International Journal of GEOMATE, May, 2017, Vol. 12, Issue 33, pp. 8-13
Geotec., Const. Mat. & Env., ISSN:2186-2990, Japan, DOI: http://dx.doi.org/10.21660/2017.33.2535

NUMERICAL SIMULATION OF DESICCATION CRACKING PROCESS BY WEAK COUPLING OF DESICCATION AND FRACTURE

*Sayako Hirobe[1] and Kenji Oguni[2]

[1,2] Department of System Design Engineering, Keio University, Japan

*Corresponding Author, Received: 09 March 2016, Revised: 17 July 2016, Accepted: 29 Nov. 2016

ABSTRACT: The prediction of the possibilities for the desiccation cracking is important for the building construction because they could cause damages to the foundation structures. While the experimental and numerical researches were performed with various materials and conditions, the mechanism of the desiccation cracking is still not clear. In this research, the desiccation cracking is modeled by the coupling of the desiccation governed by the diffusion equation, the deformation, and the fracture. We perform the weak coupling analysis of the finite element analysis for the desiccation and the analysis of Particle Discretization Scheme Finite Element Method (PDS-FEM) for the deformation and the fracture. The simulation is carried out with the different thickness of the desiccation layer under various boundary conditions. The simulation results show the satisfactory agreement with the experimental observation in terms of the crack pattern with net-like structure, pattern formation process, and the change in size of the cells framed by the cracks depending on the thickness of the desiccation layer. This agreement between the simulation results and the experimental observations indicates that the coupling of desiccation, deformation, and fracture is a fundamental mechanism of the desiccation cracking.

Keywords: Desiccation Cracks, Pattern Formation, Coupled Problem, PDS-FEM

1. INTRODUCTION

The prediction of the possibilities for the desiccation cracking is important for the building construction because they could cause damages to the foundation structures. While the experimental and numerical researches were performed with various materials and conditions, the mechanism of the desiccation cracking is still not clear.

The results of the previous experimental researches show that the desiccation cracking has geometric features conserved in various materials and conditions [1]-[4]. For instance, the desiccation cracking has a net-like structure and forms polygonal cells framed by the cracks. The size and the shape of the cells change depending on the constraint conditions and the thickness of the specimen.

In the previous numerical approaches, some models and numerical methods are proposed to reproduce these geometric features of the desiccation cracking [5]-[8]. While these models and methods can reproduce the net-like crack patterns, they cannot reproduce the increase of the cell size depending on the thickness of the specimen or the change in crack pattern depending on the constraint conditions.

In this paper, the desiccation cracking is modeled by the coupling of the desiccation governed by the diffusion equation, the deformation, and the fracture. This model can reflect the inhomogeneous water distribution due to desiccation on the problem of the deformation and the fracture. We perform the weak coupling analysis of the finite element analysis for the desiccation and the analysis of Particle Discretization Scheme Finite Element Method (PDS-FEM) [9], [10] for the deformation and the fracture. The simulation results are compared with the experimental results qualitatively.

2. MATHEMATICAL MODEL OF DESICCATION CRACKING

The desiccation process in the mixture of the powder and the water is described by the diffusion equation in terms of the volumetric water content θ when the moisture diffusion coefficient D is assumed as constant and the gravitational effect is neglected. Consider a permeable and linearly elastic body Ω with external boundary Γ^1. When the water evaporates from the boundary Γ^1, the water distribution in Ω is given by the next initial boundary value problem:

$$\frac{\partial \theta}{\partial t} = D\nabla^2\theta \qquad \boldsymbol{x} \in \Omega \tag{1a}$$

$$D\frac{\partial \theta}{\partial \boldsymbol{n}} = -Q^1(\theta) \qquad \boldsymbol{x} \text{ on } \Gamma^1 \tag{1b}$$

$$\theta(\boldsymbol{x},0)=\bar{\theta} \qquad \boldsymbol{x}\in\Omega \tag{1c}$$

where $Q^1(\theta)$ is a water flux due to the evaporation from the boundary Γ^1 and θ is a function of the position $\boldsymbol{x}$ and time t . Here, only the liquid water movement is considered.

For the coupling of the desiccation and the fracture, the effect of the cracks should be embedded in the desiccation problem. In this research, the crack surface Γ^2 is considered as a newly created evaporation surface and a shield for the permeable flow. The evaporation from the crack surface Γ^2 can be introduced as an additional Neumann boundary condition of the initial boundary value problem for the desiccation process Eq. (1):

$$D\frac{\partial\theta}{\partial\boldsymbol{n}}=-Q^2(\theta) \qquad \boldsymbol{x}\ \text{on}\ \Gamma^2 \tag{2}$$

where $Q^2(\theta)$ is a water flux from the crack surface Γ^2 due to the evaporation.

The shield for the permeable flow can be expressed as the elimination of the water flux normal to the crack surface Γ^2. The Darcy's low in the orthonormal coordinate system $\{\boldsymbol{e}_i\}$ is

$$\boldsymbol{J}=-D\nabla\theta \tag{3}$$

where $\boldsymbol{J}$ is a water flux vector in the coordinate system $\{\boldsymbol{e}_i\}$. We define the orthonormal coordinate system $\{\boldsymbol{e}_i'\}$ with $\boldsymbol{e}_3'$ in the normal direction of the crack surface Γ^2. The projection of $\boldsymbol{J}$ on Γ^2 (denoted as $\boldsymbol{J}^c$) in the coordinate system $\{\boldsymbol{e}_i\}$ is expressed as

$$J_i^c=T_{ji}P_{jk}T_{kl}J_l \tag{4}$$

where the coordinate transform matrix T_{ij} and the projection matrix which eliminates the water flux normal to Γ^2 are

$$T_{ij}=\boldsymbol{e}_i'\cdot\boldsymbol{e}_j \tag{5}$$

$$P_{ij}=\begin{cases}1 & \text{if } i=j=1,2\\ 0 & \text{otherwize.}\end{cases} \tag{6}$$

The introduction of $\boldsymbol{J}^c$ in the place of $\boldsymbol{J}$ corresponds to the introduction of the anisotropic moisture diffusion coefficient in the initial boundary value problem Eq. (1) and the Neumann boundary condition Eq. (2) on the crack surfaces. We solve this initial boundary value problem for the water movement Eq. (1) with the Neumann boundary condition Eq. (2) on the crack surfaces by the ordinary FEM with the linear tetrahedral elements.

For the coupling of the desiccation and the deformation, the volume shrinkage corresponding to the change in the volumetric water content θ should be embedded in the deformation problem. The relationship between the change in volumetric water content θ and the volumetric drying shrinkage strain ε^v is

$$\varepsilon^v(\boldsymbol{x},t)=\frac{1}{\alpha}\frac{\rho_w}{\rho_d}\{\theta(\boldsymbol{x},0)-\theta(\boldsymbol{x},t)\} \tag{7}$$

where α is a moisture shrinkage coefficient of the powder, ρ_w is a mass density of the water, and ρ_d is a dry bulk density of the powder. When Ω is homogeneous and isotropic, the drying shrinkage strain ε_{ij}^s is

$$\varepsilon_{ij}^s=\begin{cases}\dfrac{1}{3}\varepsilon^{\mathrm{v}} & \text{if } i=j\\ 0 & \text{if } i\neq j\,.\end{cases} \tag{8}$$

In the case of the desiccation crack phenomenon, the total strain ε_{ij} can be divided into the elastic strain ε_{ij}^e and the drying shrinkage strain ε_{ij}^s. The shrinkage strain ε_{ij}^s does not contribute to the generation of the stress and the strain energy. Therefore, the stress-strain relationship and the strain energy I for the deformation problem become

$$\sigma_{ij}=c_{ijkl}(\varepsilon_{kl}-\varepsilon_{kl}^s) \tag{9}$$

$$\mathrm{I}=\int_\Omega\frac{1}{2}\left(\varepsilon_{ij}-\varepsilon_{ij}^s\right)c_{ijkl}\left(\varepsilon_{kl}-\varepsilon_{kl}^s\right)dV \tag{10}$$

where σ_{ij} is a stress tensor and c_{ijkl} is an elastic tensor.

In this paper, the analysis of the deformation and the fracture is performed by PDS-FEM. For the evaluation of the functional I in Eq. (10), PDS-FEM applies the particle discretization for the field variables with a pair of the conjugate geometries; Voronoi tessellations $\{\Phi^\alpha\}$ and Delaunay tessellations $\{\Psi^\beta\}$. The Delaunay tessellation is a tetrahedron on the three-dimensional problem. The detailed discretization scheme is shown in Oguni *et al.* [10]. Then, the discretized strain energy I is

$$\hat{\mathrm{I}}=\sum_{\beta=1}^{M}\frac{1}{2}\left(\varepsilon_{ij}^\beta-\varepsilon_{ij}^{s\beta}\right)c_{ijkl}^\beta\left(\varepsilon_{kl}^\beta-\varepsilon_{kl}^{s\beta}\right)\Psi^\beta \tag{11}$$

where M is the number of Delaunay blocks and Ψ^β is the volume of the β-th Delaunay blocks. The

displacement u_i^{α} minimizing the discretized strain energy Eq. (11) is satisfying the equation of the force equilibrium:

$$\sum_{\gamma=1}^{N} K_{ik}^{\alpha\gamma} u_k^{\gamma} = f_i^{\alpha} \tag{12}$$

where

$$K_{ik}^{\alpha\gamma} = \sum_{\beta=1}^{M} B_j^{\beta\alpha} c_{ijkl}^{\beta} B_l^{\beta\gamma} \Psi^{\beta} \tag{13}$$

$$\varepsilon_{ij}^{\beta} = \sum_{\alpha=1}^{N} \frac{1}{2} (B_j^{\beta\alpha} u_i^{\alpha} + B_i^{\beta\alpha} u_j^{\alpha}) \tag{14}$$

$$f_k^{\alpha} = \sum_{\beta=1}^{M} \varepsilon_{ij}^{s\beta} \left(c_{ijkl}^{\beta} B_l^{\beta\alpha} \right) \Psi^{\beta}. \tag{15}$$

Here, N is the number of Volonoi blocks. Once the traction on the boundary of Voronoi blocks reaches to the tensile strength, the interaction between the Voronoi blocks is lost. This loss of the interaction is introduced by changing $B_i^{\beta\alpha}$ (and thus stiffness matrix $K_{ij}^{\beta\gamma}$).

3. NUMERICAL ANALYSIS

We perform the weak coupling analysis of the finite element analysis for the desiccation and the analysis of PDS-FEM for the deformation and the fracture. The FEM analysis for the desiccation process is carried out with a constant time step Δt=0.1 hour. Then, the analysis for the deformation and the fracture is performed by PDS-FEM at each time step. When the maximum traction among all elements reaches to the 97% of the tensile strength, the time step is reduced to Δt=0.01 hour to capture the effect of the fracture surfaces on the desiccation and the deformation promptly.

3.1 One-dimensional Crack Pattern

In the case of the desiccation test on bars in Peron *et al.* [4], the mixture of water and clayey silt is shaped in a thin rectangular bar and the bar is dried on the plate. The bottom surface of the bar is constrained in the long side direction only by the notches on the plate. In this test, the cracks formed on the top surface are parallel to each other and normal to the long side.

In this paper, we perform the simulation to reproduce this experimental result. The model size and the parameters for the simulations are determined from the experiments of Peron *et al.* [4]; see Table 1. The water evaporates from the top surface and the sides of the model. The initial volumetric water content is 72.1% (constant) and the desiccation proceeds until the averaged volumetric water content reaches to the 32.4% (the averaged volumetric water content at which the crack propagation terminated in the desiccation test of Peron *et al.* [4]). The nodal displacement of the bottom surface of the model is constrained in the long side direction and the vertical direction. We prepared the finite element model with the unstructured mesh (the number of the elements is 56,597 and the number of nodes is 11,822).

Table 1 The model size and the parameters for the simulation of one-dimensional crack pattern

Model size	300 × 50 × 12 mm
Soil dry density ρ_d	2.77×10^3 kg/m^2 hour
Evaporation speed on Γ^1	2.0×10^{-4} m/hour
Evaporation speed on Γ^2	1.0×10^{-4} m/hour
Moisture shrinkage coefficient α	0.64
Moisture diffusion coefficient D	3.6×10^{-6} m^2/hour
Poisson's ratio	0.3
Young's modulus	5.0 MPa
Tensile strength	0.45 MPa

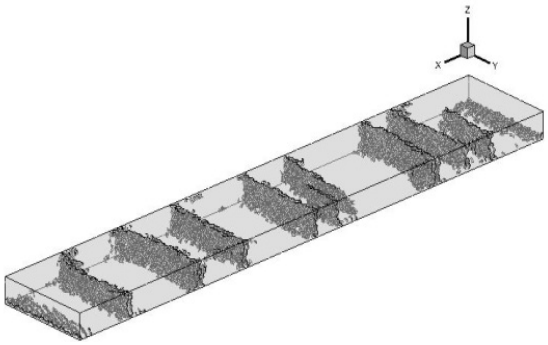

Fig. 1 Simulation result of the one-dimensional crack pattern

The simulation result (Fig. 1) shows the final crack pattern formed in the analysis model. The all cracks are parallel to each other and normal to the long side. The geometric feature of the cracks and the number of cracks formed on the top surface of the analysis model coincide with the experimental observation of Peron *et al.* [4].

3.2 Two-dimensional Crack Pattern

3.2.1 Drying tests for the comparison with simulation results of two-dimensional crack pattern

We perform the drying tests of calcium carbonate slurry to observe the crack patterns corresponding to the thickness of the specimen and to measure the parameters for the simulation of two-dimensional crack pattern. The calcium carbonate slurry was prepared at volumetric water content 72%. The slurry was poured into the rectangular acrylic container (100×100×50 mm). The thickness of the specimen was set as 5 mm, 10 mm, 20 mm, and 30 mm. The slurry was dried in the air (20 °C temperature and at 50 % relative humidity) until the specimen dried out completely.

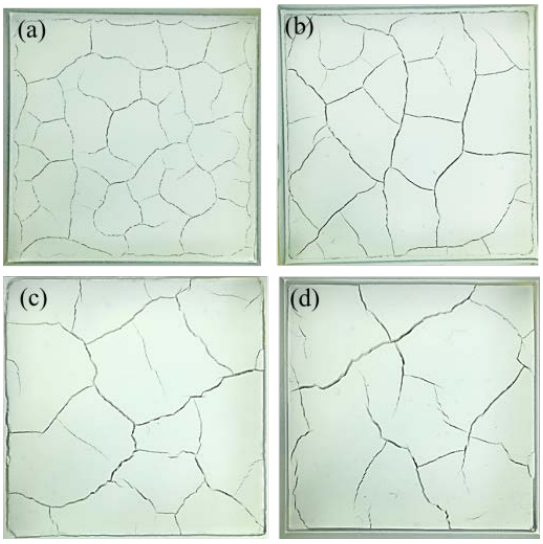

Fig.2 Final crack pattern on the top surface of the specimen formed in the drying tests. (a) 5 mm, (b) 10 mm, (c) 20 mm, and (d) 30 mm

The excessive water layer disappeared at the volumetric water content 56.0% and the crack initiated at the volumetric water content 22.4%. The crack propagation terminated at the volumetric water content 20.4%. Figure2 shows the final crack patterns on the top surface of the specimen with different thickness. The cracks with net-like structure form the polygonal cells framed by the cracks and the averaged size of the cells increases with the increase of the specimen thickness. As shown in Fig. 3, in the crack pattern formation process, some long cracks initiate on the edge of the specimen and traverse the specimen at the initial stage of the desiccation cracking. Then, relatively short cracks appear to tessellate the lager cells. These cracks often branch and terminate when they meet the existing cracks.

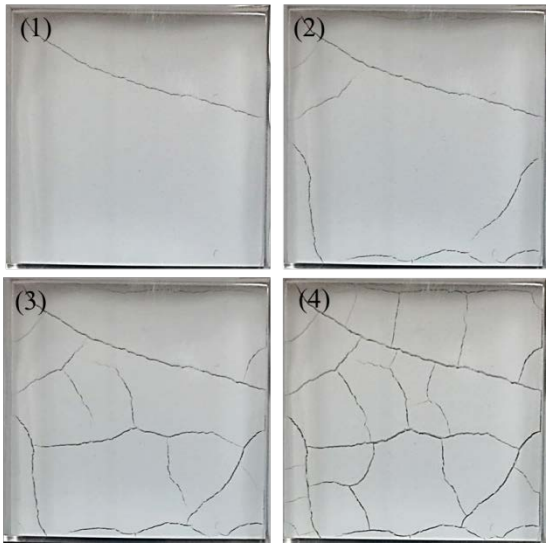

Fig.3 Crack propagation process of the drying test in the case of 10 mm thickness

3.2.2 The simulation of two-dimensional crack pattern

We perform the simulation to reproduce the two-dimensional crack pattern observed in the drying test of calcium carbonate slurry. The width and the height of the model is set as 100 mm and the depth was set as 5 mm, 10 mm, 20 mm, and 30 mm. The parameters for the simulation of two-dimensional crack pattern are shown in Table 2. The water evaporates from the top surface of the model and the nodal displacement on the sides and bottom surface of the model is constrained. The initial volumetric water content is 56.0% (constant) and the desiccation proceeds until the averaged volumetric water content reaches to the 20.4%. We prepared the finite element model with the unstructured mesh; the mesh sizes are shown in Table 3.

The final crack pattern on the top surface model with different thickness is shown in Fig.4. The cracks have a net-like structure and form polygonal cells. The cell sizes are almost constant on each thickness and the averaged cell size increases with the increase of the model thickness. These geometric features of the crack patterns and the increasing tendency of the averaged cell size qualitatively coincide with the observation of the drying experiments of the calcium carbonate slurry shown in Fig.2. In the crack pattern formation process, some long cracks extend traversing the top surface. Then, relatively short cracks propagate to tessellate the lager cells. This hierarchical sequence of the cell formation can be also observed in the drying tests of calcium carbonate slurry.

Table 2 The parameters for the simulation of two-dimensional crack pattern

Soil dry density ρ_d	800 kg/m^2 hour
Evaporation speed on Γ^1	8.8×10^{-5} m/hour
Evaporation speed on Γ^2	1.0×10^{-5} m/hour
Moisture shrinkage coefficient α	0.69
Moisture diffusion coefficient D	3.6×10^{-6} m^2/hour
Poisson's ratio	0.3
Young's modulus	5.0 MPa
Tensile strength	1.6 MPa

Table 3 The mesh sizes for the simulation of two-dimensional crack pattern

model size [mm]	number of nodes	number of elements
100×100×5	253,930	50,355
100×100×10	278,337	51,726
100×100×20	309,509	55,304
100×100×30	347,551	61,146

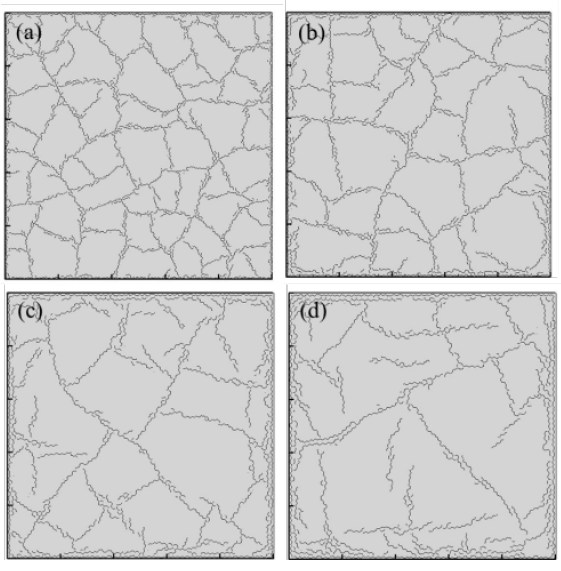

Fig.4 The final crack pattern on the top surface of the specimen formed in the simulation. (a) 5mm, (b) 10mm, (c) 20mm, and (d) 30mm

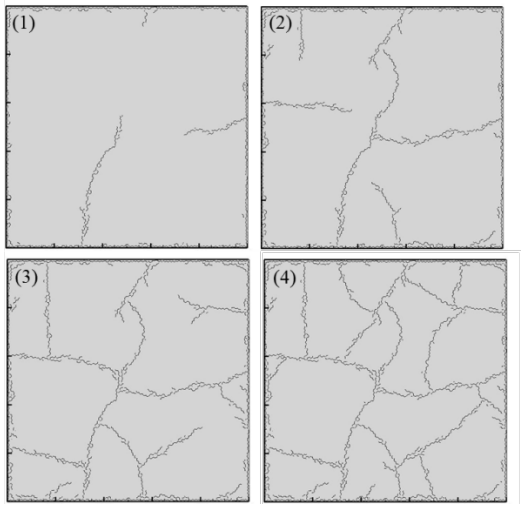

Fig.5 The crack propagation process of the drying test in the case of 10 mm thickness

4. CONCLUSION

In this paper, the coupling model of desiccation, deformation, and fracture is proposed. The simulation for the one-dimensional crack pattern and two-dimensional crack pattern is performed based on this model and the results of the simulation of the two-dimensional crack pattern are compared with the results of the drying test of calcium carbonate slurry. The simulation results show the satisfactory agreement with the experimental observation in terms of the crack pattern with net-like structure, pattern formation process, and the change in the size of the cells framed by the cracks depending on the thickness of the desiccation layer. This agreement between the simulation results and the experimental observations indicates that the coupling of desiccation, deformation, and fracture is a fundamental mechanism of the desiccation cracking.

5. REFERENCES

[1] A. Groisman and E. Kaplan, "An experimental study of cracking induced by desiccation", Europhysics. Letters. Vol. 25, 2006, pp. 415-420.

[2] H. Nahlawi and J.K. Kodikara, "Laboratory experiments on desiccation cracking of thin soil layers", Geotechnical and Geological Engineering. Vol. 24, 2006, pp. 1641-1664.

[3] H.J. Vogel, H. Hoffmann, A. Leopold and K. Roth, "Studies of crack dynamics in clay soil II. A physically based model for crack

formation", Geoderma. Vol.125, 2005, pp. 213-223.

[4] H. Peron, T. Hueckel, L. Laloui and L.B. Hu, "Fundamentals of desiccation cracking of fine-grained soils: experimental characterisation and mechanisms identification", Canadian Geotechnical Journal. Vol. 46, 2009, pp. 1177-1201.

[5] G. Musielak and T. Śliwa, "Fracturing of clay during drying: modelling and numerical simulation", Transp Porous Med. Vol. 95, 2012, pp. 465-481.

[6] J.Sima, M. Jiang and C. Zhou, "Numerical simulation of desiccation cracking in thin clayey layer using 3D discrete element modelling", Computers and Geotechnics. Vol. 56, 2014, pp. 168-180.

[7] R. Rodríguez, M. Sánchez, A. Ledesman and A. Lloret, "Experimental and numerical analysis of desiccation of mining waste", Canadian Geotechnical Journal. Vol. 44, 2007, pp. 644-658.

[8] H. Peron, J.Y. Delenne, L. Laloui and M.S. El Youssoufi, "Discrete element modelling of drying shrinkage and cracking of soils", Computers and Geotechnics. Vol. 36, 2008, pp. 61-69.

[9] M. L. L. Wijerathne, K. Oguni and M. Hori, "Numerical analysis of growing crack problems using particle discretization scheme", International Journal for Numerical Methods in Engineering, Vol. 80, 2009, pp. 46-73.

[10] K. Oguni, M.L.L. Wijerathne, T. Okinaka and M. Hori, "Crack propagation analysis using PDS-FEM and comparison with fracture experiment", Mechanics of Materials. Vol. 41, 2009, pp. 1242-1252.